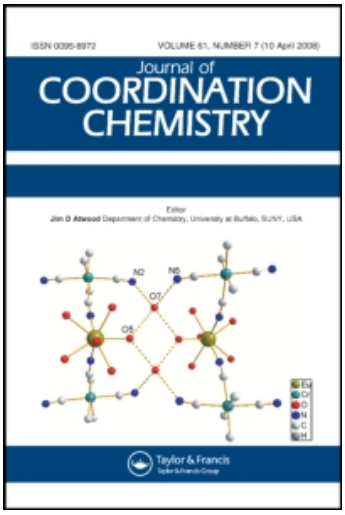

Journal of Coordination Chemistry
Publication details, including instructions for authors and subscription information:
http://www.informaworld.com/smpp/title~content=t713455674

REDOX AND pH-INDUCED SWITCHING OF THE COORDINATION SITES IN THE 3-HYDROXYPICOLINATE RUTHENIUM(III)-edta COMPLEX

Francisca N. Rein[a]; Reginaldo C. Rocha[a]; Henrique E. Toma[a]
[a] Institute de Química, Universidade de São Paulo, São Paulo, SP, Brazil

To cite this Article Rein, Francisca N. , Rocha, Reginaldo C. and Toma, Henrique E.(2001) 'REDOX AND pH-INDUCED SWITCHING OF THE COORDINATION SITES IN THE 3-HYDROXYPICOLINATE RUTHENIUM(III)-edta COMPLEX', Journal of Coordination Chemistry, 53: 2, 99 — 123
To link to this Article: DOI: 10.1080/00958970108022606
URL: http://dx.doi.org/10.1080/00958970108022606

J. Coord. Chem., 2001, Vol. 53, pp. 99–123
Reprints available directly from the publisher
Photocopying permitted by license only

REDOX AND pH-INDUCED SWITCHING OF THE COORDINATION SITES IN THE 3-HYDROXYPICOLINATE RUTHENIUM(III)-edta COMPLEX

FRANCISCA N. REIN, REGINALDO C. ROCHA and HENRIQUE E. TOMA*

Instituto de Química, Universidade de São Paulo, Caixa Postal 26077, CEP 05599-970 São Paulo, SP, Brazil

(Received 2 March 2000; In final form 14 July 2000)

Ruthenium(III)-edta reacts with the 3-hydroxypicolinate ligand ($Hhpic^-$) at pH 5, yielding the practically colorless $[Ru^{III}(edta)(\kappa N, \kappa O\text{-}Hhpic)]^{2-}$ complex (H_2hpic = 3-hydroxypicolinic acid; H_4edta = ethylenedinitrilotetraacetic acid). Above pH 9, deprotonation of the phenolic group promotes an intramolecular linkage isomerization process, generating the faint red $[Ru^{III}(edta)(\kappa O, \kappa O\text{-}hpic)]^{3-}$ complex. Both isomers can be electrochemically reduced, converting into a single deep red $[Ru^{II}(edta)(\kappa N, \kappa O\text{-}Hhpic)]^{3-}$ complex strongly stabilized by ruthenium-to-pyridinecarboxylate $d_\pi \rightarrow p_\pi^*$ charge-transfer interactions. The observed distinct binding properties as a function of the oxidation states and pH have been rationalized based on semiempirical theoretical calculations for the complexes.

Keywords: Ruthenium-edta complex; 3-hydroxypicolinic acid; Linkage isomerism; Cyclic voltammetry; Spectroelectrochemistry

1. INTRODUCTION

The coordination chemistry of ruthenium-edta with polyfunctional species such as the 3-hydroxypicolinate ion ($Hhpic^-$ or $hpic^{2-}$) is characterized by the existence of several variable binding modes in the ligand, imposing a

*Corresponding author. Tel.: 55 11 3818 3887, Fax: 55 11 3815 5579, e-mail: henetoma@iq.usp.br

challenge for the elucidation of the nature of products generated as a function of the pH and metal ion oxidation states. This type of study is relevant from the point of view of coordination chemistry, since polyfunctional ligands are widespread in nature, and the investigation of their binding properties can be of great usefulness, particularly for understanding the role of the metal ions in biological systems.

The 3-hydroxypicolinic acid can undergo a series of acid–base equilibria, as shown in Scheme 1, involving the protonation/deprotonation of the carboxylate group, the pyridine ring and the phenolate group, according to $pK_a(1) = 1.14$, $pK_a(2) = 5.19$ and $pK_a(3) = 12.01$, respectively [1, 2]. In basic medium, it can bind metal ions *via* the pyridine and carboxylate groups, in a bidentate mode, as in the related picolinate ligand [3–6]; or *via* the phenolic and carboxylate groups, as in the salicylate ligand [7–9]. In the case of ruthenium-edta, the binding modes were found to depend on the oxidation states, as well as, on the pH. A detailed investigation on this system is reported, based on spectroscopic, kinetics, electrochemical and spectro-electrochemical techniques.

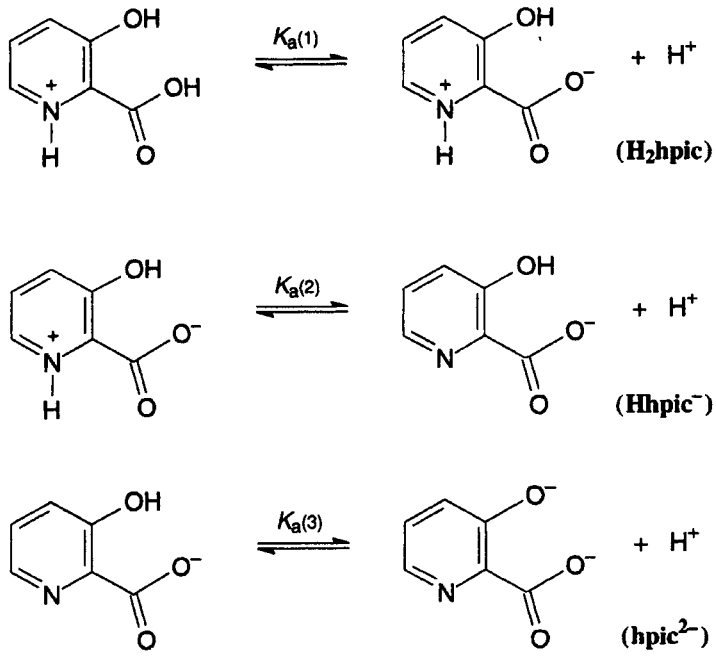

SCHEME 1

2. EXPERIMENTAL

2.1. Syntheses

$[Ru^{III}(H_2edta)(Hhpic)] \cdot 5H_2O$ was synthesized by reacting 0.0685 g (0.148 mmol) of $Ru^{III}(Hedta)(H_2O)$ [10, 11] and 0.0228 g (0.164 mmol) of 3-hydroxypicolinic acid (Aldrich), in 25 mL of water. After stirring for 10 min, a yellowish precipitate appeared. The solid was collected on a filter, washed with ethanol and kept under vacuum. Yield: 67%. Anal. Calcd. for $C_{16}H_{28}N_3O_{16}Ru$ (%): C, 31.0; H, 4.7; N, 6.8. Found: C, 30.5; H, 4.6; N, 7.1.

The deprotonated complexes, $[Ru^{III}(edta)(Hhpic)]^{2-}$ and $[Ru^{III}(edta)(hpic)]^{3-}$, were prepared in solution, under an argon atmosphere by: (**a**) dissolving the yellow solid (prepared as described above) in an air-purged PIPES 0.05 M buffered solution and, then, adjusting the pH with addition of millivolumes of a 3.0 M NaOH solution (PIPES = 1,4-piperazinediethanesulfonic acid); or (**b**) reacting equimolar quantities of the starting materials ($[Ru^{III}(Hedta)(H_2O)] \cdot 3H_2O$ and 3-hydroxypicolinic acid) in buffered solutions at the required pH. For kinetic measurements, the experiments were carried out under *pseudo*-first order conditions (ligand concentrations at least 10 times in excess).

The reddish deprotonated complex, $Na_3[Ru^{III}(edta)(hpic)] \cdot 4H_2O$, was also isolated by adding dichloromethane to a concentrated solution of the protonated complex in a water/methanol (1 : 2) mixture, after titrating with a 3.0 M NaOH solution. The solid was collected on a filter and kept under vacuum. Yield: around 80%. Anal. Calcd. for $C_{16}H_{23}N_3O_{15}Na_3Ru$ (%): C, 28.8; H, 3.5; N, 6.3. Found: C, 29.1; H, 3.9; N, 6.5.

2.2. Physical Measurements

The electronic spectra of the aqueous solutions of the compounds were recorded on a Hewlett-Packard model 8453 diode-array spectrophotometer. Cyclic voltammetry measurements were carried out with a Princeton Applied Research instrument consisting of a model 283 potentiostat, using a conventional electrochemical cell containing a glassy carbon working electrode, a Ag/AgCl (1.0 M KCl) reference electrode (0.222 V *versus* SHE) and a platinum wire auxiliary electrode. The supporting electrolyte used was 0.1 M NaTFA (where NaTFA = sodium trifluoroacetate). The spectroelectrochemical measurements were carried out as described elsewhere [12, 13]. Magnetic susceptibility measurements were performed at 293 K, on a Cahn model 7500 electrobalance, using a 5000 G magnet.

X-band EPR spectra were recorded on a Bruker model ER 200D-SRC spectrometer, operating at 9.45 GHz, at 77 K.

The pK_a values were determined by spectrophotometric or potentiometric measurements as a function of pH. In the former case, cells were specially designed in order to combine simultaneous pH measurements with absorption spectra. pH measurements were carried out with a model MD21 digital pH meter from Digimed. Kinetic measurements were carried out using an Applied Photophysics stopped-flow instrument. The data acquisition and processing were run with use of the software package provided by Applied Photophysics. The solutions were always freshly prepared, under an argon atmosphere, using 0.10 M NaTFA to keep constant the ionic strength. All the measurements were carried out at 298 K.

2.3. Molecular Calculations and Computational Details

Semiempirical molecular orbital calculations were carried out by using Zerner's spectroscopic implementation of the INDO (Intermediate Neglect of Differential Overlap) method [14] (ZINDO/S) within the HyperChem 5.1 program from Hypercube, Inc. (Gainesville, FL, USA, 1998). The default parameterization was based on the original ZINDO program package [15]. As interaction factors, the universal values $k_{p\sigma}=1.267$ and $k_{p\pi}=0.585$ were used. SCF molecular orbitals were obtained at the RHF (Restricted Hartree-Fock) level. Geometry optimizations for the ligand and the complexes were carried out as necessary using the AM1 [16–18] and ZINDO/1 methods with its resident parameters. The electronic spectra simulation (singly excited configuration interaction, SECI, within an active space involving ten occupied and ten unoccupied molecular orbitals) and the atomic charge distribution were obtained from the ZINDO/S calculations, for both free ligand or ruthenium complexes. Initial nuclear coordinates of the molecules were given by molecular mechanics calculations employing the MM+ module, a modified MM2 force field [19] from HyperChem, with a gradient of 1×10^{-5} kcal Å^{-1} mol^{-1} as a convergence criterion in a conjugate gradient algorithm. All the calculations were performed on a PC Windows platform with a Pentium III microprocessor.

3. RESULTS AND DISCUSSION

3.1. Electronic Structure of the 3-hydroxypicolinate Ligand

The electronic spectra of the 3-hydroxypicolinic acid are shown in Figure 1. At pH 4, the predominant form corresponds to the *N*-protonated neutral

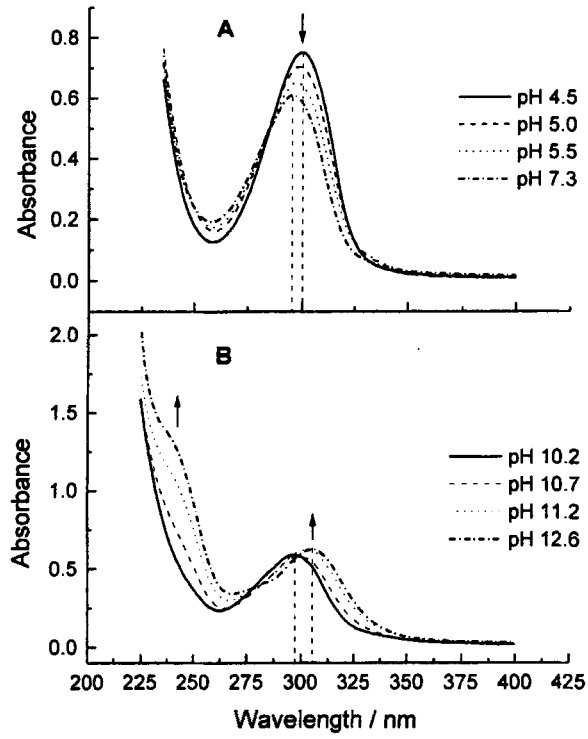

FIGURE 1 Electronic spectra of the 3-hydroxypicolinic acid as a function of the pH, showing the deprotonation equilibria involving the pyridinium group ($pK_a = 5.3$) and the deprotonation of the phenolic group ($pK_a = 11.5$).

species (**H_2hpic**; Scheme 1), exhibiting a strong pyridine $\pi \rightarrow \pi^*$ band at 300 nm ($\varepsilon = 7500\,M^{-1}\,cm^{-1}$). As one increases the pH from 4.5 to 7.3, this band shifts to 295 nm, and is accompanied by a small decrease of intensity ($\varepsilon = 6100\,M^{-1}\,cm^{-1}$), reflecting the deprotonation of the pyridinium center. The calculated pK_a from the spectrophotometric data was 5.3, in agreement with the literature [2]. Above pH 10, the UV band undergoes a bathochromic shift to 310 nm ($\varepsilon = 5800\,M^{-1}\,cm^{-1}$) and a new shoulder appears at 240 nm (ca. $8900\,M^{-1}\,cm^{-1}$), as a consequence of the deprotonation of the aromatic —OH group. The calculated $pK_a = 11.5$ is also consistent with the literature [2].

The observed changes in the electronic spectra can be explained based on ZINDO/S semiempirical theoretical calculations for the **H_2hpic**, **Hhpic**$^-$ and **hpic**$^{2-}$ species. The relevant HOMO and LUMO levels are represented by the molecular orbitals labeled from MO number 23 to MO number 28, whose corresponding three-dimensional orbital representations and eigenvalues are shown in the Figure 2.

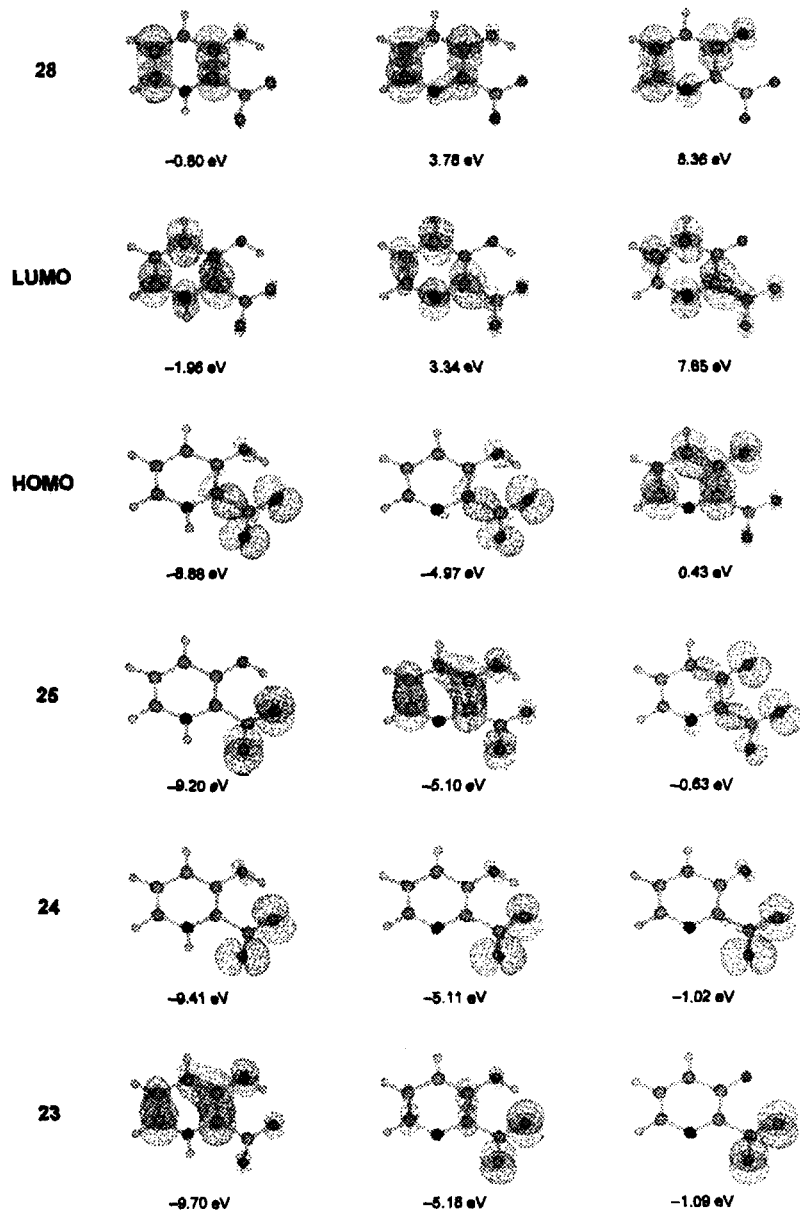

FIGURE 2 ZINDO plots of the main ground state HOMO and LUMO frontier levels and its eigenvalues for the H_2hpic, $Hhpic^-$ and $hpic^{2-}$ species. (See Color Plate I at the back of the journal).

As one can see in that figure, the HOMO (MO no. 26) levels of H_2hpic and Hhpic$^-$ are mainly localized on the carboxylate sites. It is interesting to note that the occupied MO levels no. 23 and 25 are predominantly centered on the pyridine ring in the H_2hpic and Hhpic$^-$ molecules, respectively, exhibiting a nodal plane at the *N*-atom. On the other hand, the deprotonation of the aromatic —OH group has a dramatic effect on the frontier levels, making that pyridine ring delocalized orbital into the highest-energy occupied molecular orbital and leading to a greater contribution of the phenolate-side region in the hpic^{2-} species. It is interesting to note that in all cases the LUMO (MO no. 27) levels are mainly localized on the pyridine ring with some contribution of the carboxylate group. These π-acceptor levels are expected to be of great relevance in the interaction of π-backbonding species, such as the Ru(II) ions.

The calculated electronic transitions for the partially (H_2hpic and Hhpic$^-$) and the totally deprotonated (hpic^{2-}) ligands are shown in Table I, in comparison with the experimental ones. The reasonable agreement supports the assignment, in terms of molecular orbitals, of those bands in the UV region to the electronic transitions from occupied π-MOs (MO no. 23 [HOMO − 2], 25 [HOMO − 1] and 26 [HOMO]) to unoccupied π^*-MOs (MO no. 27 [LUMO] and 28 [LUMO + 1]) in those species (see Tab. I).

The total charge density for the Hhpic$^-$ and hpic^{2-} ligands are shown in Figure 3. For the Hhpic$^-$ ligand, the atomic charge distribution is mainly concentrated on the carboxylate group, indicating that it is the major binding site for metal ions. In the case of the hpic^{2-} ligand, the charge distribution is concentrated on the phenolate and carboxylate groups, supporting their preferential coordination to metal ions.

3.2. Ruthenium(edta)-(3-hydroxypicolinate) Complexes

The formation of the ruthenium(III)-(edta)-(3-hydroxypicolinate) complex was strongly dependent on the pH. At pH 4.7, the ligand is in the Hhpic$^-$

TABLE I Experimental and theoretical spectra for the lower-energy $\pi \rightarrow \pi^*$ electronic transitions in the (a) H_2hpic, (b) Hhpic$^-$, and (c) hpic^{2-} ligands

	Experimental		*Calculated*		*Transition*
Species	λ (*nm*)	ε (M^{-1} cm^{-1})	λ (*nm*)	*osc. strength*	$MO_i \rightarrow MO_f$
a	300	7500	304	0.315	#23 → #27
b	295	6100	288	0.165	#25 → #27
c	310	5800	320	0.363	#26 → #27
	240	8900	255	0.577	#26 → #28

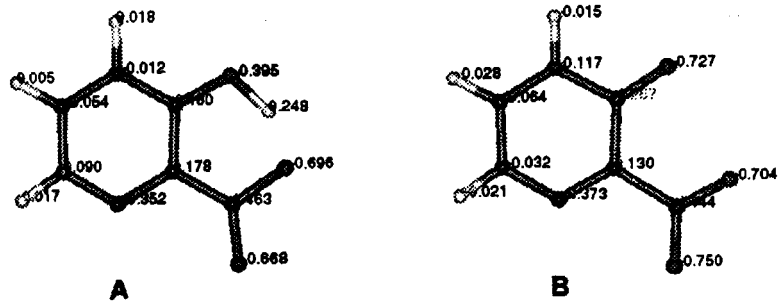

FIGURE 3 Total charge distribution in the $Hhpic^-$ and $hpic^{2-}$ molecules. (See Color Plate II at the back of the journal).

form, exhibiting a carboxylate group and a pyridine *N*-atom available for binding to the Ru^{III}(edta) complex. Except for an absorption shoulder around 370 nm and a ligand $\pi \rightarrow \pi^*$ band at 300 nm ($\varepsilon = 16400\,M^{-1}\,cm^{-1}$), the yellow complex generated by mixing equimolar amounts $[Ru^{III}(edta)(H_2O)]^-$ and $Hhpic^-$ (3×10^{-3} M) did not display any characteristic band in the visible region, as one can see in Figure 4. At pH 10.0, however, the ligand is in the $hpic^{2-}$ form, and two new absorption bands appeared in the electronic spectra of the red complex, at 495 nm ($\varepsilon = 1200\,M^{-1}\,cm^{-1}$) and 350 nm ($6500\,M^{-1}\,cm^{-1}$) in addition to the $\pi \rightarrow \pi^*$ transitions at 295 and 250 nm.

The acid–base titration curve for the ruthenium(III)-(edta)-(3-hydroxypicolinic) complex exhibited two well defined inflections corresponding to the deprotonation of the pyridine ring and the phenolic group. The calculated pK_a values for the coordinated ligand in the complex were 3.5 and 7.9, respectively. A similar spectrophotometric titration was carried out in the range of pH 4.7 to 11, leading to an equilibrium constant of $1.26 \times 10^{-8}\,M^{-1}$ for the deprotonation of the phenolic group.

$$[Ru^{III}(edta)(Hhpic)]^{2-} \rightleftharpoons [Ru^{III}(edta)(hpic)]^{3-} + H^+$$

$$K_a = 1.26 \times 10^{-8}\,M^{-1}$$

The best evidence for formation of the $[Ru^{III}(edta)(Hhpic)]^{2-}$ complex was provided by cyclic voltammetry and spectroelectrochemical measurements shown in Figures 5 and 6, respectively. At pH 4.7, a reversible pair of waves was obtained, exhibiting $E_{1/2} = 0.17$ V *vs.* SHE, corresponding to the $Ru^{III/II}$ redox couple. This wave can be readily differentiated from that of the starting $[Ru^{III/II}(edta)(H_2O)]^-$ species ($E_{1/2} = -0.010$ V) [20]. As the pH was increased from 4.7 to 10.0, a systematic decay of the initial waves at 0.17 V occurred in parallel with the rise of a new wave at 0.00 V. This new

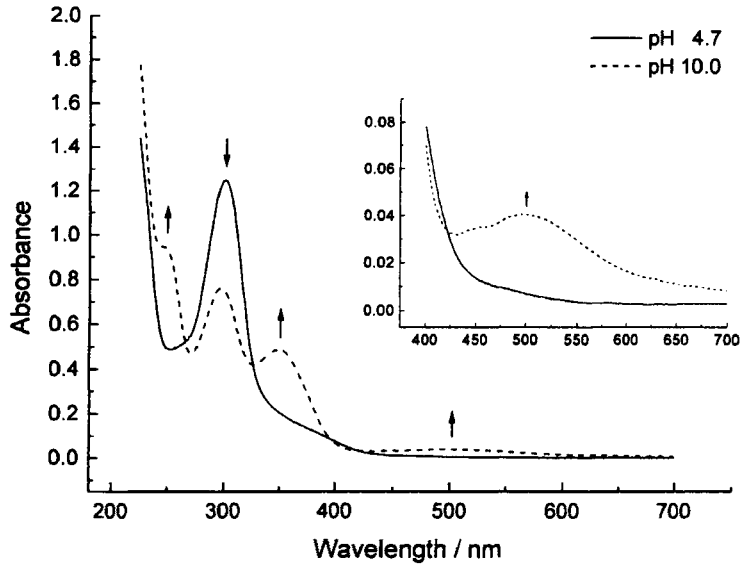

FIGURE 4 Electronic spectra of aqueous solutions containing an equimolar mixture of Ru^{III}(edta) and 3-hydroxypicolinic acid at concentrations of 3.0×10^{-3} M (length = 0.025 cm; pH values are indicated in the figure).

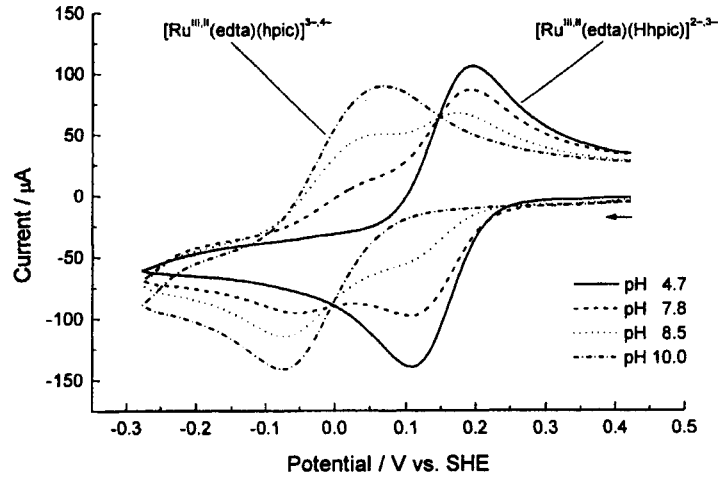

FIGURE 5 Cyclic voltammograms of the ruthenium(III)-(edta)-(3-hydroxypicolinate) complex obtained at the pH range from 4.7 to 10.0 (concentration = 3.0×10^{-3} M; ionic strength = 0.1 M NaTFA; scan rate = 200 mV s^{-1}).

wave cannot be ascribed to the $[Ru^{III/II}(edta)(H_2O)]^{-/2-}$ system, since these species are practically colorless, and the observed product at pH > 9 is typically red.

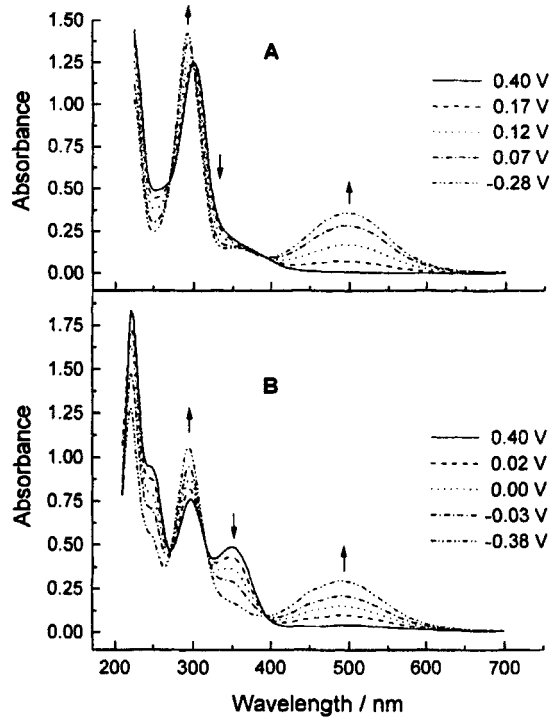

FIGURE 6 Spectroelectrochemistry of the ruthenium(III)-(edta)-(3-hydroxypicolinate) complex in an aqueous solution at pH 4.7 (A) and 10.0 (B) (concentration = 3.0×10^{-3} M; ionic strength = 0.1 M NaTFA; length = 0.025 cm).

In general, acid–base equilibrium corresponds to a rapid process, leading to a systematic shift of the observed wave as a function of pH, with no evidence of isosbestic points in the cyclic voltammograms [21]. In contrast, the observed changes (Fig. 5) are consistent with an equilibrium process involving two distinct species. It has been observed, *e.g.*, at pH 8.0, that the two waves respond in a different way, to the changes in the rates and in the direction of the scanning applied potentials, indicating that the equilibrium reaction proceeds within the time scale of the cyclic voltammograms, in contrast to the conventional acid–base reactions.

The spectroelectrochemical measurements carried out for the system are illustrated in Figure 6. At pH 4.7, the reduction of the pale yellow $[Ru^{III}(edta)(Hhpic)]^{2-}$ complex was typically Nernstian, with $E^0 = 0.17$ V *vs.* SHE, leading to the formation of a deep red product displaying an absorption band at 500 nm ($\varepsilon = 4600\,M^{-1}\,cm^{-1}$). Only a small bathochromic shift (from 300 to 293 nm; both with $\varepsilon = 1.6 \times 10^4\,M^{-1}\,cm^{-1}$) was

observed for the $Hhpic^-$ $\pi \rightarrow \pi^*$ transitions in the UV region. At pH 10, a Nernstian behavior was also observed at $E^0 = 0.00$ V, converting the reddish $[Ru^{III}(edta)(hpic)]^{3-}$ complex into the same deep red product observed at pH 4.7.

From the spectroelectrochemical results it is evident that the starting Ru^{III} complexes at pH 4.7 and 10.0 consist of two different species in equilibrium, but a single reduced (Ru^{II}) complex is generated in both situations. Therefore, the reduced species generated at pH 10.0 should undergo a complete conversion to the red product observed at pH 4.7, during the time scale of the spectroelectrochemical measurements ($\sim$ 5 min).

In order to elucidate this puzzling behavior, we carried out a comparative study with the related picolinate (**pic**) and salicylate (**sal**) ruthenium-edta complexes (see Scheme 2), since they exhibit the complementary parts involved in the 3-hydroxypicolinate system.

The starting material $[Ru^{III}(edta)(H_2O)]^-$ reacted with the picolinate ligand yielding a colorless complex in the pH range 4.5–9.0. In addition to the $\pi \rightarrow \pi^*$ bands in the picolinate ligands, only a new absorption shoulder was observed around 350 nm, as in the case of the $Hhpic^-$ complex. Potentiometric titrations for this complex exhibited only a single inflection, corresponding to a $pK_a = 3.5$, associated with the pyridine ring. The cyclic voltammograms for this complex were not pH dependent in the range 4.7–10.0, exhibiting a reversible wave at $E_{1/2} = 0.18$ V *vs.* SHE, which is very close to that observed for the $Hhpic^-$ complex (at pH 4.7). In the reduced form, a deep red product was observed, exhibiting a strong absorption band at 492 nm ($4050\ M^{-1}\ cm^{-1}$). The results are very similar to those observed for the $[Ru^{III/II}(edta)(Hhpic)]^{2-/3-}$ system at pH 4.7 (Tab. II).

On the other hand, the reaction of ruthenium(III)-edta with salicylate can be monitored above pH 10, by the rise of a weak, but characteristic band at 530 nm, very similar to that observed for the $[Ru^{III}(edta)(hpic)]^{3-}$ complex under identical conditions. A single wave was observed in the cyclic voltammograms, at $E_{1/2} = -0.42$ V *vs.* SHE (Tab. II). In contrast, however,

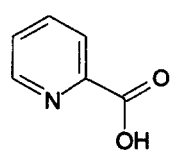

(Hpic)

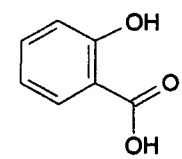

(H_2sal)

SCHEME 2

TABLE II Spectroscopic and electrochemical data for the Ru-edta derivatives with the Hhpic$^-$, hpic^{2-}, pic$^-$, and sal^{2-} ligands

Complex	*CT (LM or ML)* λ_{max}/nm	*Internal L* λ_{max}/nm	$Ru^{III/II}$ *redox pair* $E_{1/2}/V$ *vs. SHE*
$[Ru^{III}(edta)(Hhpic)]^{2-}$	–(*)	300 (16400)	0.17
$[Ru^{II}(edta)(Hhpic)]^{3-}$	500 (4600)	293 (16500)	0.17
$[Ru^{III}(edta)(pic)]^{2-}$	–(*)	258 (12300)	0.18
$[Ru^{II}(edta)(pic)]^{3-}$	492 (3650) 391 (3000)	261 (13200)	0.18
$[Ru^{III}(edta)(hpic)]^{3-}$	495 (1200)	295 (10300) 350 (6500)	0.00
$[Ru^{II}(edta)(hpic)]^{3-}$	–(**)	–(**)	0.00
$[Ru^{III}(edta)(sal)]^{3-}$	530 (1350)	296 (7200)	−0.42
$[Ru^{II}(edta)(sal)]^{3-}$	–(**)	–(**)	−0.42

(*) No absorption CT bands in the visible region; (**) Data not available; the reduced species dissociates.

the reduction of the $[Ru^{III}(edta)(sal)]^{3-}$ complex does not lead to a deep red product. Instead, dissociation takes place, releasing the colorless $[Ru^{II}(edta)(H_2O)]^{2-}$ complex and the salicylate ligand.

Therefore, one can conclude that, at pH 4.7, the ruthenium(III) complex should be coordinated to the pyridine-carboxylate group, as in the picolinate ligand. This complex can be represented as $[Ru^{III}(edta)(\kappa N, \kappa O\text{-Hhpic})]^{2-}$. Above pH 8–9, this species isomerizes to the carboxy-phenolate derivative $[Ru^{III}(edta)(\kappa O, \kappa O\text{-hpic})]^{3-}$, displaying a similar spectrum to that observed for the corresponding salicylate complex (see Scheme 3). In the reduced form, the ruthenium(II) species exists as the pyridine-carboxylate isomer $[Ru^{II}(edta)(\kappa N, \kappa O\text{-Hhpic})]^{3-}$, in the pH range from 4.5 to 10.0.

3.3. Theoretical Calculations and Molecular Orbital Analysis

In order to understand the electronic properties of the two isomers, theoretical calculations were carried out using the spectroscopic implementation

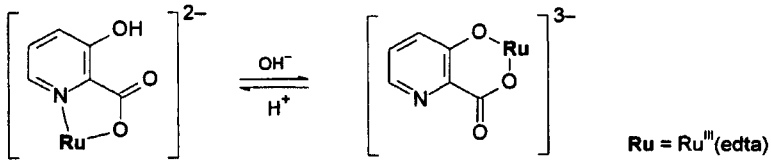

SCHEME 3

of the ZINDO method and Restricted Hartree-Fock theory (*vide infra*). Since crystallographic data for these systems are not available, the nuclear coordinates of the complexes used in the ZINDO/S calculations were obtained from MM+ geometry optimizations using atomic charges from ZINDO/1 single point calculations (both Restricted and Unrestricted Hartree-Fock theories were used, depending on the oxidation state of the metal ion: Ru^{II} and Ru^{III}, respectively). The procedure involving mixed methods at different levels of calculation (namely, ZINDO/1 and MM+) was repeated several times for each molecule, up to the global energy minimum convergence. The theoretical structures for the oxidized *N,O* and *O,O*-isomer species are illustrated in Figure 7, and the more relevant information about the structural data related to these complexes are shown in Table III. In general, the representative bond distances and angles involving the central metal ion are very close to the reported X-ray crystallographic data for the Ru^{III}(Hedta)(H_2O) complex [22].

The relevant energy levels and molecular orbital contributions and the theoretical spectrum calculated by ZINDO/S were collected in Tables IV and V, respectively, for the $[Ru^{III}(edta)(\kappa N, \kappa O\text{-Hhpic})]^{2-}$, $[Ru^{III}(edta)(\kappa O, \kappa O\text{-hpic})]^{3-}$ and $[Ru^{II}(edta)(\kappa N, \kappa O\text{-Hhpic})]^{3-}$ complexes. In addition, the frontier orbitals (SOMO or HOMO and LUMO) surface plots for these complexes are shown in Figure 8.

According to the ZINDO results, the highest-energy populated levels (SOMO or HOMO) are metal-centered in both isomer species and redox states, although they present mixed character (see discussion below). On the other hand, the nature of the lowest-energy unpopulated levels (LUMO) is associated essentially with the 3-hydroxypicolinate ligands. Another observation deals with the composition of the wave functions related to the ligand-centered orbitals. While the frontier MOs are primarily composed of the ruthenium metal (*e.g.*, 3 OMOs) and the polyfunctional $Hhpic^-$ or $hpic^{2-}$ ligands (*e.g.*, 2 or 3 UMOs), the more internal or external populated or unpopulated MOs have the mixing contribution of the edta co-ligand enhanced, with participation reaching almost the totality of the orbital representation (see Tab. IV).

The main difference between the $[Ru^{III}(edta)(\kappa N, \kappa O\text{-Hhpic})]^{2-}$ and $[Ru^{III}(edta)(\kappa O, \kappa O\text{-hpic})]^{3-}$ isomers is associated with the composition of their LUMOs (Tabs. IVA and IVB, respectively; LUMO #87), since the *N,O*-species possesses considerable orbital mixing (with smaller metallic character) while the analogous *O,O*-species practically does not present any contribution from the ruthenium d_π orbitals in its lowest-energy unpopulated π^* orbital. This reflects the importance of the π-backdonation

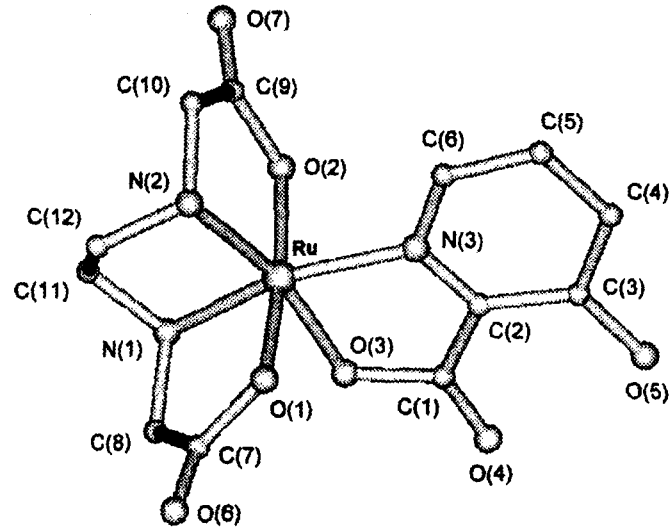

A

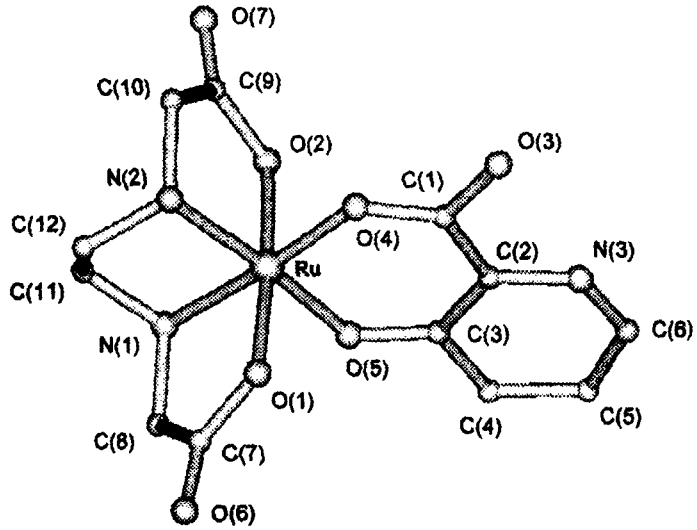

B

FIGURE 7 Core geometry optimized molecular structures (MM+/ZINDO1) of the (A) $[Ru^{III}(edta)(\kappa N, \kappa O\text{-Hhpic})]^{2-}$ and (B) $[Ru^{III}(edta)(\kappa O, \kappa O\text{-hpic})]^{3-}$ (the free acetate groups and the hydrogens atoms were omitted for a better clarity; full molecular structures of the complexes are represented in Fig. 8).

TABLE III Selected calculated bond distances (Å) and angles (°) for the molecules of the (A) $[Ru^{III}(edta)(\kappa N, \kappa O\text{-Hhpic})]^{2-}$, and (B) $[Ru^{III}(edta)(\kappa O, \kappa O\text{-hpic})]^{3-}$ complexes

Bond distance	*A*	*B*	*Angle*[a]	*A*	*B*
Ru—O(1)	1.893	1.893	O(1)—Ru—O(3)	81.98	–
Ru—O(2)	1.891	1.893	O(1)—Ru—O(5)	–	87.91
Ru—N(1)	1.987	2.007	O(1)—Ru—N(1)	85.78	86.88
Ru—N(2)	1.994	2.003	O(1)—Ru—N(2)	86.97	90.13
Ru—O(3)	1.909	–	O(1)—Ru—N(3)	99.71	–
Ru—O(4)	–	1.821	O(1)—Ru—O(4)	–	95.31
Ru—N(3)	1.959	–	O(2)—Ru—O(3)	105.45	–
Ru—O(5)	–	1.820	O(2)—Ru—O(5)	–	94.68
O(1)—C(7)	1.353	1.341	O(2)—Ru—N(3)	84.72	–
N(1)—C(8)	1.467	1.465	O(2)—Ru—O(4)	–	88.21
N(1)—C(11)	1.460	1.460	O(2)—Ru—N(1)	92.71	89.46
O(3)—C(1)	1.351	1.368	O(2)—Ru—N(2)	85.33	87.05
N(3)—C(2)	1.266	1.271	N(1)—Ru—N(2)	89.02	89.36
N(3)—C(6)	1.265	1.263	N(1)—Ru—O(3)	82.17	–
O(4)—C(1)	1.216	1.260	N(1)—Ru—O(5)	–	86.97
O(5)—C(3)	1.361	1.258	N(2)—Ru—N(3)	114.06	–
O(6)—C(7)	1.214	1.212	N(2)—Ru—O(4)	–	87.79
C(1)—C(2)	1.348	1.398	O(3)—Ru—N(3)	75.97	–
C(2)—C(3)	1.399	1.398	O(5)—Ru—O(4)	–	95.95
C(3)—C(4)	1.398	1.400	O(1)—Ru—O(2)	172.17	175.40
C(4)—C(5)	1.394	1.394	N(1)—Ru—N(3)	156.40	–
C(5)—C(6)	1.397	1.394	N(1)—Ru—O(4)	–	176.41
C(7)—C(8)	1.510	1.506	N(2)—Ru—O(3)	166.32	–
C(11)—C(12)	1.527	1.528	N(2)—Ru—O(5)	–	175.93

[a] Only angles involving the metal-coordinated internal atoms and having the Ru ion as the intermediate atom between two bonds.

interaction, which is pronounced for the *N,O*-isomers; it is particularly evident in the reduced species (Tab. IVC), that shows almost twice the metallic character (attributed to the $d_\pi - p_\pi^*$ interactions) in relation to the oxidized one.

One more complicated situation can be seen in the $[Ru^{III}(edta)(\kappa N, \kappa O\text{-Hhpic})]^{2-}$ OMOs mixing (Tab. IVA), that reveals an elevated degree of covalency with an unexpected contribution of the edta co-ligand. The SOMO level (MO #86) presents contributions very similar to the corresponding reduced species and the *O,O*-isomer (Tabs. IVC and IVB; MO #86). However, the lower-energy Ru d_π orbitals (namely d_{xz} and d_{xy}) are completely mixed with the edta character, as well as the edta levels are very mixed with the metal character. Assignment of this kind of behavior is not an easy task, but it could be understood as an effect of the energy lowering of the redox levels, as a consequence of the metal oxidation state (see the MO energies – Tab. IVA – for this Ru^{III} *N,O*-isomer in comparison with those for the reduced Ru^{II} *N,O*-species – Tab. IVC – and the Ru^{III} *O,O*-isomer – Tab. IVB), coupled to the relatively high-energy

TABLE IV. Energy levels and wavefunction composition of some frontier molecular orbitals of the (A) $[Ru^{III}(edta)(\kappa N, \kappa O\text{-Hhpic})]^{2-}$, (B) $[Ru^{III}(edta)(\kappa O, \kappa O\text{-hpic})]^{3-}$ and (C) $[Ru^{II}(edta)(\kappa N, \kappa O\text{-Hhpic})]^{3-}$ complexes

MO index	*Energy (eV)*	*Ru (%)*	*(H)hpic (%)*	*edta (%)*
		A		
91	5.863	1.83	2.22	95.95
90	5.639	0.39	0.71	98.90
89	5.301	1.49	97.22	1.29
88	3.784	0.61	99.15	0.24
87 (LUMO)	3.151	7.73	90.59	1.68
86 (SOMO)	−0.259	63.29[a]	18.39	18.32
85	−3.233	21.42[b]	2.95	75.63
84	−3.295	39.03[c]	5.10	55.86
79	−3.868	46.64[d]	9.11	44.26
78	−4.164	21.25[e]	6.77	71.98
		B		
91	9.384	0.44	98.72	0.83
90	9.034	0.81	0.83	98.36
89	8.944	0.96	0.34	98.70
88	7.879	0.76	98.89	0.35
87 (LUMO)	7.059	0.58	99.31	0.11
86 (SOMO)	3.712	67.43[f]	15.26	17.31
85	0.904	63.59[g]	18.15	18.26
84	0.205	72.75[h]	23.02	4.23
83	−0.917	0.06	0.45	99.49
82	−1.048	2.82	55.05	42.14
		C		
91	9.257	0.98	2.27	96.75
90	8.999	0.72	0.56	98.72
89	8.871	1.29	95.61	3.10
88	7.246	1.52	98.14	0.34
87 (LUMO)	6.714	13.14[i]	84.25	2.61
86 (HOMO)	1.508	59.70[j]	23.86	16.44
85	1.182	68.31[k]	11.04	20.66
84	0.574	80.95[l]	11.79	7.26
83	−0.759	0.08	0.15	99.76
82	−0.902	0.01	0.02	99.97

[a] 55.4% Ru d_{yz};
[b] 17.8% Ru d_{xz};
[c] 31.8% Ru d_{xz};
[d] 32.0% Ru d_{xy};
[e] 13.7% Ru d_{xy};
[f] 40.8% Ru d_{yz} + 16.6% Ru d_{xz};
[g] 36.7% Ru d_{xz} + 19.5% Ru d_{yz};
[h] 66.9% Ru d_{xy};
[i] 5.4% Ru d_{yz};
[j] 51.6% Ru d_{yz};
[k] 55.2% Ru d_{xz} + 7.3 Ru d_{z^2};
[l] 52.9% Ru d_{xy} + 18.1 Ru $d_{x^2-y^2}$ + 7.5 Ru d_{yz}.

edta levels. In addition, the intensified split of the t_{2g} orbitals could originate from an electronic perturbation resulting from the significant structural distortion of the molecule in the equatorial plane direction, which would be provoked by the much more hindered coordination of

TABLE V. Electronic spectra (only the lowest energy transitions) of the (A) $[Ru^{III}(edta)(\kappa N,\kappa O\text{-Hhpic})]^{2-}$, (B) $[Ru^{III}(edta)(\kappa O,\kappa O\text{-Hhpic})]^{3-}$, and (C) $[Ru^{II}(edta)(\kappa N,\kappa O\text{-hpic})]^{3-}$ complexes

	Experimental		*Calculated*		
Complex	λ (*nm*)	ε ($M^{-1}cm^{-1}$)	λ (*nm*)	*osc. strength*	*Assignment*
A	370	(sh)	365	0.012	Ru ($d-d$)[a]
B	495	1200	506	0.057	LMCT
C	500	4600	515	0.161	MLCT
			505	0.114	MLCT

[a] $d-d$ transition ($t_{2g}^5e_g^0 \rightarrow t_{2g}^4e_g^1$) but with some charge transfer character.

the *N,O*-Hhpic ligand than that shown for the *O,O*-hpic ligand (see Fig. 7 and Tab. III).

One important aspect involved in the chemistry of these systems refers exactly to the charge delocalization and the orbital mixing among the metal and the ligands. This subject has been the aim of research of several recently reported studies, dealing principally with ruthenium complexes containing noninnocent ligands and/or quinone derivatives [23].

From the ZINDO analysis, one can conclude that there is a significant metal-ligand orbital mixing in the SOMO/HOMO redox levels for the three studied complexes, with approximately equal contributions of the 3-hydroxypicolinate ($Hhpic^-$ or $hpic^{2-}$) and the ethylenedinitrilotetraacetate (edta) ligands. This apparent unusual behavior for this class of polyfunctional complexes explains, from the electronic interaction point of view, the stabilization of the Ru^{II} species by coordination *via* the more π-acceptor *N,O* sites (through a π-backdonation mechanism), and the favorable *O,O* (donor sites) coordination mode observed in the deprotonated complex, in order to stabilize the Ru^{III} species. The latter observation is confirmed by the greater degree of covalency between the ruthenium and the $hpic^{2-}$ ligand in the $O,O-Ru^{III}$ species, what can be easily seen if one considers the molecular orbital mixing coefficients of the three d_π levels (Tab. IVB; #86 [SOMO], #85 [SOMO − 1] and #84 [SOMO − 2]).

Recent studies making use of ZINDO treatments of ruthenium species, with similar approaches, have shown that this method is successful in predicting molecular orbital mixing behavior and spectroscopic properties [7, 23–25]. Therefore, one can have some confidence that this method is meaningful.

3.4. Kinetics of Formation and Equilibrium Constants

The rates and equilibrium constants for the complexes were obtained from the study of the kinetics of formation of the complexes in solution. Starting

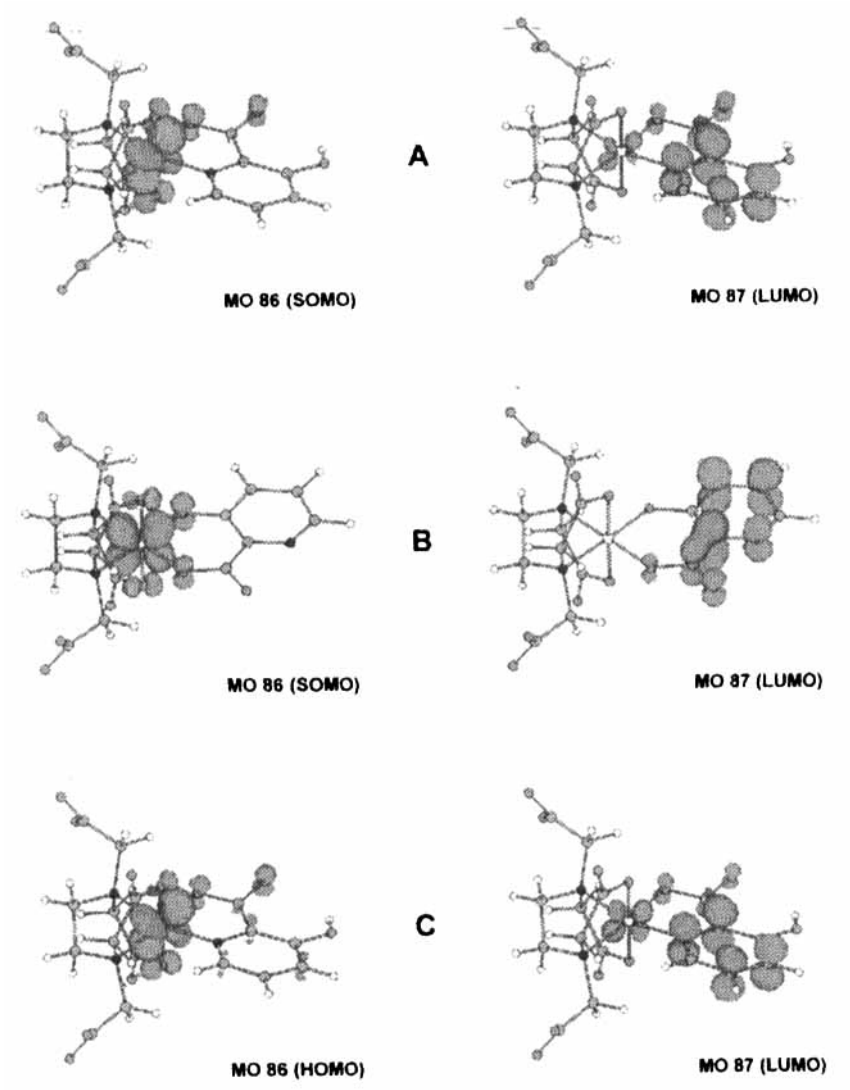

FIGURE 8 Selected frontier molecular orbitals [SOMO (Ru^{III}) or HOMO (Ru^{II}), and LUMO] of the (A) $[Ru^{III}(edta)(\kappa N, \kappa O\text{-Hhpic})]^{2-}$, (B) $[Ru^{III}(edta)(\kappa O, \kappa O\text{-hpic})]^{3-}$ and (C) $[Ru^{II}(edta)(\kappa N, \kappa O\text{-Hhpic})]^{3-}$ complexes. (See Color Plate III at the back of the journal).

from the $[Ru^{III}(edta)(H_2O)]^-$ complex, the formation of the $[Ru^{III}(edta)(\kappa N, \kappa O\text{-Hhpic})]^{2-}$ and $[Ru^{III}(edta)(\kappa N, \kappa O\text{-pic})]^{2-}$ complexes was monitored at 350 nm, leading to first order kinetics in the presence of a high excess of the $Hhpic^-$ or the pic^- ligand. The observed rate constants, in both cases, exhibited a linear dependence on the concentration of the

entering ligands, in the range of 1.0–5.0 mM. The corresponding second order rate constants (k_f) were 15.0 and 14.0 $M^{-1}s^{-1}$, respectively. Since the substitution mechanisms for $[Ru^{III}(edta)(H_2O)]^-$ are typically associative [20], the similar rate constants measured for the pic^- and $Hhpic^-$ ligands are coherent with the involvement of the same binding sites in the two complexes. It is important to note that the typical substitution rate constants for pyridine ligands are around $6 \times 10^3\ M^{-1}s^{-1}$, *i.e.*, more than two orders of magnitude higher than those observed for the pic^- and $Hhpic^-$ ligands. Therefore, one can deduce that in the substitution process, the attack of the poorly nucleophilic carboxylate groups on the $[Ru^{III}(edta)(H_2O)]^-$ complex prevails over the attack of pyridine *N*-atom, which is more strongly hindered. After this step, the intramolecular ring closure process should proceed very rapidly, since it is facilitated by the anchoring process, leading to a bidentate coordination of the ligand.

The dissociation of the pic^- and $Hhpic^-$ ligands from the complex was promoted by adding a strong binding species such as the 2-mercapto-pyridine [26] (pySH) ligand. In the presence of an excess of the attacking ligands, the formation of the $[Ru^{III}(edta)(pySH)]^-$ ($\lambda = 600$ nm) complex proceeded by first order kinetics. The observed rate constants exhibited a saturation behavior, independent of the nature of the attacking ligand, providing the intrinsic rate (k_d) for the dissociation of the coordinated $Hhpic^-$ or pic^- ligands. The values of k_d for the $[Ru^{III}(edta)(Hhpic)]^{2-}$ and $[Ru^{III}(edta)(pic)]^{2-}$ complexes were 1.8×10^{-3} and $8.0 \times 10^{-4}\ s^{-1}$, respectively.

From the kinetic constants for the formation and dissociation reactions, the corresponding equilibrium constants ($K = k_f/k_d$) for the $[Ru^{III}(edta)(Hhpic)]^{2-}$ and $[Ru^{III}(edta)(pic)]^{2-}$ complexes were calculated as 8.3×10^3 and $1.8 \times 10^4\ M^{-1}$, respectively. By solving the square thermodynamic cycle in Schemes 4 and 5, the equilibrium constants ($K_2 = K_1 \cdot \exp[nF(\Delta E)/RT]$, where $\Delta E = E_2 - E_1$, $n = 1$ and $T = 298$ K) for the reduced $Hhpic^-$

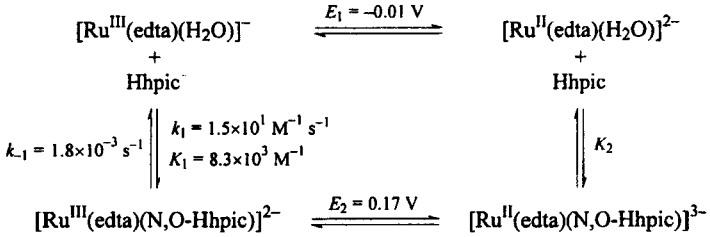

SCHEME 4

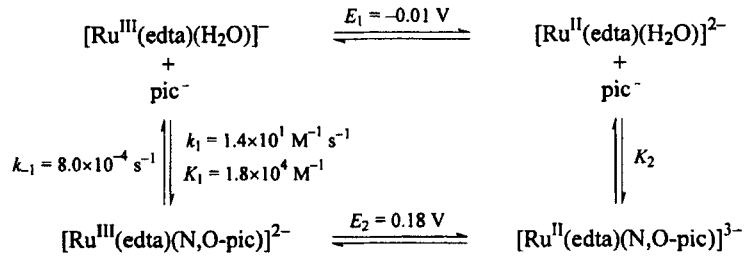

SCHEME 5

and pic^- complexes were calculated as 9.2×10^6 and $2.9 \times 10^7\,M^{-1}$, respectively.

It is evident in these cases that the pyridine-carboxylate groups stabilize preferentially the Ru^{II} oxidation state, by more than two orders of magnitude, with respect to the Ru^{III} one. As observed from the theoretical calculations, the Ru^{II} complex is a good π-donor species capable of interacting with the empty π^* orbitals of the pyridine-carboxylate ligands. This interaction is reflected in the observed metal-to-ligand charge transfer bands, and should be responsible for the stabilization of the Ru^{II} state.

3.5. Isomerization Kinetics

After the formation of the $[Ru^{III}(edta)(\kappa N, \kappa O\text{-Hhpic})]^{2-}$ complex, pH jump experiments were carried out by adding borate buffer (pH 10.0) and monitoring the linkage isomerization process at 495 nm which corresponds to the absorption band of the $[Ru^{III}(edta)(\kappa O, \kappa O\text{-hpic})]^{3-}$ complex. The observed isomerization kinetics were typically first order, as illustrated in Figure 9. The calculated kinetic constants, $k = 4.7 \times 10^{-3}\,s^{-1}$ were independent on the concentration of the $hpic^{2-}$ ligand ($8.0 \times 10^{-3} - 4.0 \times 10^{-2}\,M$), in agreement with an intramolecular isomerization process. This intramolecular process can be understood considering that after the rupture of the Ru—N(pyridine) bond, the attached ruthenium(III) complex can undergo a rapid rotation through the carboxylate group in order to bind to the phenolate site. According to the cyclic voltammograms of Figure 5, the isomerization equilibrium is completely shifted in the direction of the $[Ru^{III}(edta)(\kappa O, \kappa O\text{-hpic})]^{3-}$ complex, since there is no evidence for the $[Ru^{III}(edta)(\kappa N, \kappa O\text{-hpic})]^{3-}$ isomer around $E = 0.17\,V$ *vs.* SHE, at pH 10.0.

As the acid–base equilibrium constant involving the $[Ru^{III}(edta)(\kappa N, \kappa O\text{-Hhpic})]^{2-}$ and $[Ru^{III}(edta)(\kappa O, \kappa O\text{-hpic})]^{3-}$ species also corresponds to the

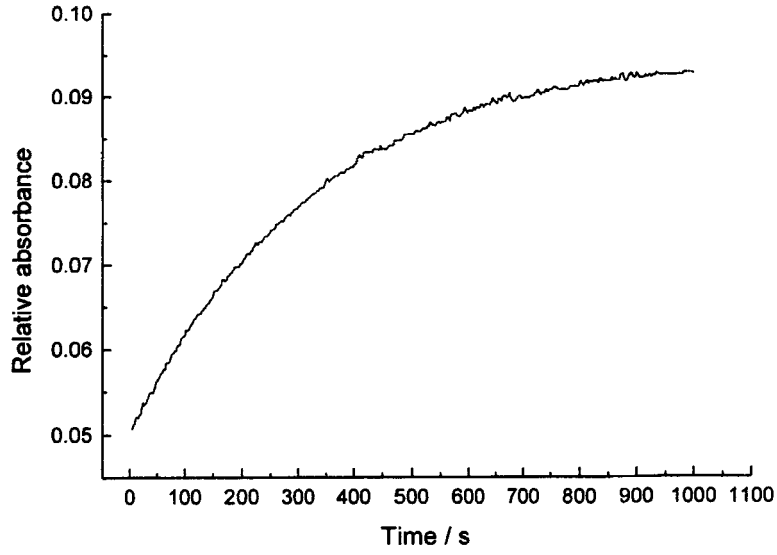

FIGURE 9 Typical isomerization kinetics for the $[Ru^{III}(edta)(\kappa N, \kappa O\text{-Hhpic})]^{2-}$ complex, at pH 10.0, monitored at 500 nm.

isomerization equilibrium constant, $K^{III}_{N,O\rightarrow O,O}$, then the analogous constant related to the reduced species may also be estimated from the square thermodynamic cycle outlined in Scheme 6. In this way, the value of $K_4 = K^{II}_{N,O\rightarrow O,O}$ was determined to be 1.7×10^{-11}, that helps to explain why the *O,O*-isomer complex is not observed in the measurements at the employed pH conditions.

3.6. Magnetism and EPR Spectra

Solid state magnetic moment measurements indicated that the complexes are one-electron paramagnets at 293 K. The presence of paramagnetic trivalent ruthenium in the solutions was also established by EPR

$$\begin{array}{ccc} [Ru^{III}(edta)(N,O\text{-Hhpic})]^{2-} & \xrightleftharpoons{E_2 = 0.17\ V} & [Ru^{II}(edta)(N,O\text{-Hhpic})]^{3-} \\ + H^+ \Big\uparrow\Big\downarrow \begin{array}{l} k_3 = 4.7\times10^{-3}\ s^{-1} \\ K_3 = 1.3\times10^{-8} \end{array} & & + H^+ \Big\uparrow\Big\downarrow K_4 \\ [Ru^{III}(edta)(O,O\text{-hpic})]^{3-} & \xrightleftharpoons{E_3 = 0.00\ V} & [Ru^{II}(edta)(O,O\text{-hpic})]^{4-} \end{array}$$

SCHEME 6

measurements. Typical EPR spectra for the $[Ru^{III}(edta)(\kappa N, \kappa O\text{-Hhpic})]^{2-}$ and $[Ru^{III}(edta)(\kappa O, \kappa O\text{-hpic})]^{3-}$ complexes, recorded at 77 K, in glassy methanol, are shown in Figure 10, for comparison purposes (the data are set out in Tab. VI). The X-band spectra are rhombic in nature with three rather distinct signals, which is characteristic of paramagnetic ruthenium(III) in a *pseudo*-octahedral symmetry environment (low-spin Ru^{III}, t_{2g}^5, $S=(1/2)$) [27–29], due to rhombic molecular distortions, exhibiting g_1, g_2 and g_3 values equal to 2.815, 2.181 and 1.582, and 2.729, 2.259 and 1.598 for the protonated (yellow) and the deprotonated (red colored) species, respectively.

It is important to notice that the observed tensor g values in this work for the systems involving the complexes with the 3-hydroxypicolinate are quite different from those reported for the starting complex $[Ru^{III}(edta)(H_2O)]^-$

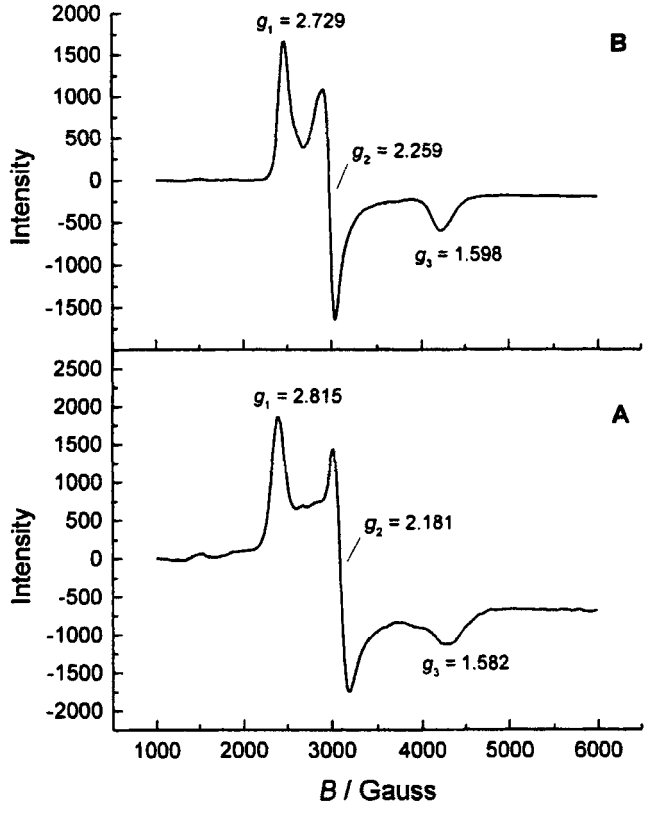

FIGURE 10 X-band EPR spectra for the (A) $[Ru^{III}(edta)(\kappa N, \kappa O\text{-Hhpic})]^{2-}$ and (B) $[Ru^{III}(edta)(\kappa O, \kappa O\text{-hpic})]^{3-}$ complexes, recorded at 77 K, in glassy methanol.

TABLE VI Magnetic moments and EPR g values for the complexes: (A) $[Ru^{III}(edta)(\kappa N, \kappa O\text{-Hhpic})]^{2-}$; (B) $[Ru^{III}(edta)(\kappa O, \kappa O\text{-hpic})]^{3-}$; and (C) $[Ru^{III}(edta)(H_2O)]^{-}$

Complex	μ_{eff}[a] (B.M.)	g values[b]		
		g_1	g_2	g_3
A	1.85	2.815	2.181	1.582
B	1.89	2.729	2.259	1.598
C[c]	-	2.393	2.345	1.765

[a] Solid state at 293 K;
[b] Glassy methanol at 77 K;
[c] Ref. [30].

[30], whose spectrum was also obtained in glassy solution at 77 K (Tab. VI). This difference in behavior reflects the change of chemical environment and magnetic field around the ruthenium(III) as a consequence of the coordination of the polyfunctional ligand, that causes the intensification of the rhombic distortion. Under the influence of lower symmetry, the d_{xy}, d_{xz} and d_{yz} orbitals split and exhibit quite different energies, allowing more separated and defined transitions between the three levels than in the essentially axial symmetry situation.

As one can see from the g values, the $[Ru^{III}(edta)(\kappa N, \kappa O\text{-Hhpic})]^{2-}$ complex is more strongly distorted than the $[Ru^{III}(edta)(\kappa O, \kappa O\text{-hpic})]^{3-}$ complex, reflecting the existence of the two different atoms in the binding sites within a more steric hindered coordination mode. In addition, the spectrum of the yellow complex $[Ru^{III}(edta)(\kappa N, \kappa O\text{-hpic})]^{2-}$, shows the appearance of a small hyperfine structure perturbation, reflecting the more pronounced contribution of the ligand in the redox Ru^{III} levels of this complex. These results are completely consistent with the MO calculations, that reveal the ruthenium nature of the redox level (singly occupied molecular orbital–SOMO) and the more mixed metal-ligand character of the frontier molecular orbitals in the $[Ru^{III}(edta)(\kappa N, \kappa O\text{-hpic})]^{2-}$ species.

4. CONCLUSION

The reaction between ruthenium(III)-edta and the 3-hydroxypicolinate ligand ($Hhpic^-$) leads to the practically colorless $[Ru^{III}(edta)(\kappa N, \kappa O\text{-Hhpic})]^{2-}$ complex. Deprotonation of the phenolic group, above pH 9, is followed by an intramolecular linkage isomerization process, generating the faint red $[Ru^{III}(edta)(\kappa O, \kappa O\text{-hpic})]^{3-}$ complex. The reduction of the two isomers leads to the deep red $[Ru^{II}(edta)(\kappa N, \kappa O\text{-Hhpic})]^{2-}$ complex,

which is strongly stabilized by ruthenium-to-pyridinecarboxylate, $d_\pi \rightarrow p^*_\pi$ charge-transfer interactions.

Acknowledgements

The support from John Simon Guggenheim Memorial Foundation (HET), and the Brazilian Agencies CNPq and FAPESP is gratefully acknowledged. We are thankful to Prof. Dr. Ohara Augusto and Dr. Edlaine Linares (Universidade de São Paulo) for the EPR measurements. We would also like to thank Prof. Dr. Luiz Antonio A. de Oliveira and Alcenir A. Santos (Universidade Estadual Paulista) for their precious help.

References

[1] ACD/I-Lab (ACD/pKa version 3.5); Advanced Chemistry Development Inc., Toronto, ON, Canada, 1998.
[2] A. K. W. Stephens and C. Orvig, *Inorg. Chim. Acta* **273**, 47 (1998).
[3] V. R. L. Constantino, L. F. C. de Oliveira, P. S. Santos and H. E. Toma, *Transition Met. Chem.* **19**, 103 (1994).
[4] N. Ghatak, J. Chakravarty and S. Bhattacharya, *Polyhedron* **14**, 3591 (1995); N. Ghatak and S. Bhattacharya, *Polyhedron* **13**, 2999 (1994).
[5] K. N. Mitra, S. Choudhury, S. Goswami and S. M. Peng, *Polyhedron* **16**, 1605 (1997).
[6] S. M. Couchman, J. M. Dominguez-Vera, J. C. Jeffery, C. A. McKee, S. Nevitt, M. Pohlman, C. M. White and M. D. Ward, *Polyhedron* **17**, 3541 (1998).
[7] V. R. L. Constantino, H. E. Toma, L. F. C. de Oliveira, F. N. Rein, R. C. Rocha and D. O. Silva, *J. Chem. Soc., Dalton Trans.*, p. 1735 (1999).
[8] A. Pramanik, N. Bag and A. Chakravorty, *J. Chem. Soc., Dalton Trans.*, p. 97 (1992).
[9] C. F. Edwards, W. P. Griffith, A. J. P. White and D. J. Williams, *J. Chem. Soc., Dalton Trans.*, p. 3813 (1993).
[10] M. Mukaida, H. Okuno and T. Ishimori, *Nippon Kagaku Zasshi* **86**, 589 (1965).
[11] Y. Oshino, T. Uehiro and M. Saito, *Bull. Chem. Soc. Jpn.* **52**, 1060 (1979).
[12] R. C. Rocha, K. Araki and H. E. Toma, *Transition Met. Chem.* **23**, 13 (1998).
[13] F. N. Rein and H. E. Toma, *Polyhedron* **17**, 1439 (1998).
[14] M. C. Zerner, G. H. Loew, R. F. Kirchner and U. T. Mueller-Westerhoff, *J. Am. Chem. Soc.* **102**, 589 (1980); A. D. Bacon and M. C. Zerner, *Theor. Chim. Acta* **53**, 21 (1979); J. E. Ridley and M. C. Zerner, *Theor. Chim. Acta* **42**, 223 (1976); J. E. Ridley and M. C. Zerner, *Theor. Chim. Acta* **32**, 111 (1973).
[15] ZINDO: A comprehensive semiempirical SCF/CI package written by M. C. Zerner, and co-workers, Quantum Theory Project, University of Florida, Gainesville, FL, USA.
[16] AM1 (Austin Model 1), a semiempirical quantum method developed by M. J. S. Dewar, and colaborators, University of Texas at Austin, USA.
[17] M. J. S. Dewar and K. M. Dieter, *J. Am. Chem. Soc.* **108**, 8075 (1986); M. J. S. Dewar, E. G. Zoebisch, E. F. Healy and J. J. P. Stewart, *J. Am. Chem. Soc.* **107**, 3902 (1985).
[18] J. J. P. Stewart, *J. Comp. Aided Mol. Design* **4**, 1 (1990).
[19] N. L. Allinger, *J. Am. Chem. Soc.* **99**, 8127 (1977).
[20] T. Matsubara and C. Creutz, *Inorg. Chem.* **18**, 1956 (1979).
[21] S. Wawzonek, In: *Physical Methods of Chemistry*, A. Weissberger and B. W. Rossiter, Eds. (Wiley-Interscience, New York, 1971), Part IIA, Chapter I.
[22] K. Okamoto, J. Hidaka, I. Iida, K. Higashino and K. Kanamori, *Acta Cryst.* **C46**, 2327 (1990).

[23] R. A. Metcalfe and A. B. P. Lever, *Inorg. Chem.* **36**, 4762 (1997) and references therein.
[24] M. D. Ward, *Inorg. Chem.* **35**, 1712 (1996).
[25] Y. K. Shin, B. S. Brunschwig, C. Creutz, M. D. Newton and N. Sutin, *J. Phys. Chem.* **100**, 1104 (1996).
[26] H. E. Toma, P. S. Santos, M. P. D. Mattioli and L. A. A. Oliveira, *Polyhedron* **6**, 603 (1987).
[27] K. J. LaChance-Galang, P. E. Doan, M. J. Clarke, U. Rao, A. Yamano and B. Hoffman, *J. Am. Chem. Soc.* **117**, 3529 (1995).
[28] B. M. Holligan, J. C. Jeffery, M. K. Norgett, E. Schatz and M. D. Ward, *J. Chem. Soc., Dalton Trans.*, p. 3345 (1992).
[29] A. Pramanik, N. Bag, G. K. Lahiri and A. Chakravorty, *J. Chem. Soc., Dalton Trans.*, p. 3823 (1990); G. K. Lahiri, S. Bhattacharya, M. Mukherjee, A. K. Mukherjee and A. Chakravorty, *Inorg. Chem.* **26**, 3359 (1987).
[30] D. Chatterjee, H. C. Bajaj and A. Hussain, *J. Coord. Chem.* **31**, 329 (1994).